Applied Catalysis B: Environmental 130–131 (2013) 270–276

Contents lists available at SciVerse ScienceDirect

Applied Catalysis B: Environmental

journal homepage: www.elsevier.com/locate/apcatb

One-pot synthesis of gold nanoparticle/molybdenum cluster/graphene oxide nanocomposite and its photocatalytic activity

Alexandre Barras[a], Manash R. Das[b], Rami Reddy Devarapalli[c], Manjusha V. Shelke[c], Stéphane Cordier[d], Sabine Szunerits[a], Rabah Boukherroub[a,*]

[a] Institut de Recherche Interdisciplinaire (IRI, USR CNRS 3078), Université Lille 1, Parc de la Haute Borne, 50 Avenue de Halley, BP 70478, 59658 Villeneuve d'Ascq, France
[b] Materials Science Division, CSIR-North East Institute of Science and Technology, Jorhat 785 006, Assam, India
[c] Physical and Materials Chemsitry Division, CSIR-National Chemical Laboratory, Pune 411 008, India
[d] Université de Rennes 1, Institut Sciences Chimiques de Rennes, UR1-CNRS 6226, Equipe Chimie du Solide et Matériaux, Campus de Beaulieu, CS 74205, 35042 Rennes Cedex, France

ARTICLE INFO

Article history:
Received 24 July 2012
Received in revised form 9 November 2012
Accepted 12 November 2012
Available online 24 November 2012

Keywords:
$[Mo_6Br_8(N_3)_6]^{2-}$ cluster
Graphene oxide
Gold nanoparticles
Nanohybrid
Rhodamine B
Photodegradation
Visible light

ABSTRACT

The paper reports on a facile one-pot synthesis of a tri-component gold nanoparticle/molybdenum cluster/graphene oxide (AuNPs@Mo–GO) nanohybrid composite. The synthetic methodology consists on direct UV irradiation of an aqueous solution containing graphene oxide (GO), $Na_2[Mo_6Br_8(N_3)_6]$, $HAuCl_4{\cdot}3H_2O$ and isopropanol at room temperature in air using a UV fiber lamp. The composite material exhibits very high photocatalytic activity for the degradation of rhodamine B under visible light irradiation. The resulting nanohybrid material was characterized using Raman spectroscopy, UV–vis spectrometry, transmission electron microscopy (TEM) and X-ray photoelectron spectroscopy (XPS).

1. Introduction

The use of synthetic dyes in many fields of applications such as textiles, papers, leathers, additives, food and cosmetics is continuously increasing. Due to their extensive applications, large-scale production and chemical stability, these pollutants can cause significant environmental pollution [1].

A wide range of methods such as photocatalysis have been developed and extensively studied for the removal of hazardous chemical compounds from water wastes to decrease their impact on the environment. Even though much work in heterogeneous photocatalysis has been focused on semiconductor materials such as TiO_2, ZnO, Fe_2O_3, WO_3, Ta_2O_5, ZnS and CdS, these materials often display large bandgaps, which require UV light irradiation and thus limiting the efficient utilization of solar energy [2].

Recently, we have demonstrated the high photocatalytic performance of the molybdenum cluster compound, $Na_2[Mo_6Br_8(N_3)_6]$, for the degradation of organic pollutants under visible and solar light irradiation [3]. Molybdenum atom octahedral clusters are nanosized molecular units that exhibit a large absorption window from UV to visible and a large emission window from red to infrared due to the delocalization of valence electrons on all metal centers [4–6].

Graphene oxide (GO), obtained by chemical treatment of graphite powder with strong chemical oxidants, has found widespread applications in various fields [7–9]. In the last years, there has been a huge interest in the literature to integrate metal nanoparticles onto GO and reduced graphene oxide (rGO) surfaces for the preparation of graphene-based nanohybrid materials [10]. The resulting nanocomposites have shown excellent properties and improved functionalities due to the synergetic effects between GO and the inorganic components. For example, Zhang et al. [11] reported that GO can be reduced via a direct redox reaction in the presence of Sn^{2+} and Ti^{3+} cations to form rGO–SnO_2 and rGO–TiO_2 composites with a good photocatalytic performance for the degradation of rhodamine B under visible light irradiation. Xiong et al. [12] demonstrated that rGO-gold nanocomposites displayed an excellent visible-light photocatalytic activity for the degradation of rhodamine in water.

The aim of the present work is to take advantage of the exceptional properties of GO and the excellent photocatalytic performance of $Na_2[Mo_6Br_8(N_3)_6]$ for the preparation of a new class of composite materials. Herein, we report on a simple and facile synthetic methodology for the preparation of a tri-component

* Corresponding author. Tel.: +33 3 62 53 17 24; fax: +33 3 62 53 17 01.
E-mail address: rabah.boukherroub@iri.univ-lille1.fr (R. Boukherroub).

0926-3373/$ – see front matter © 2012 Elsevier B.V. All rights reserved.
http://dx.doi.org/10.1016/j.apcatb.2012.11.017

AuNPs@Mo–GO nanohybrid. In this method, an aqueous solution containing GO, $Na_2[Mo_6Br_8(N_3)_6]$, $HAuCl_4{\cdot}3H_2O$ and isopropanol was irradiated at room temperature in air using a UV fiber lamp. The tri-component material was found to exhibit high photocatalytic activity for the degradation of rhodamine B under visible light irradiation.

2. Experimental part

2.1. Preparation of $Na_2[Mo_6Br_8(N_3)_6]$

500 mg of NaN_3 were introduced in an Schlenk container with 20 mL of methanol at 55 °C. After dissolution of NaN_3, 1 g of $MoBr_2$ was added to the solution. After one night of reaction, a clear solution was obtained. After filtration and evaporation of methanol, $Na_2[Mo_6Br_8(N_3)_6]$ was separated from excess of NaN_3 and NaBr by 3 successive extractions with dry acetone. Yield: 74%. EDS Na: 12; Mo: 41; Br: 47 (theo: 12.5/37.5/50). The presence of N_3 on the cluster was confirmed by IR analysis [13].

2.2. Preparation of AuNPs@Mo–GO nanocomposite

GO nanosheets investigated in this work are prepared by the modified Hummer's method from natural graphite powder according to recently published work [14–17].

In a typical procedure, an aqueous solution of GO (600 μL, 1.5 mg mL^{-1}), $Na_2[Mo_6Br_8(N_3)_6]$ (600 μL, 1 mM), $HAuCl_4{\cdot}3H_2O$ (600 μL, 1.5 mM), and isopropanol (4 μL) was irradiated at λ = 365 nm (power intensity = 0.5 W cm^{-2}) for 30 min at room temperature in air using a UV fiber lamp (Spot Light Source 300–450 nm, L9588-01, Hamamatsu, Japan). The AuNPs@Mo–GO material was separated from the solution by centrifugation (14 000 rpm for 20 min). The product was washed with water several times and resuspended in water at a concentration of 1 mg mL^{-1}.

2.3. Photodegradation of RhB under visible light irradiation

The catalytic properties of the AuNPs@Mo–GO nanocomposite have been evaluated for the photocatalytic degradation of rhodamine B (RhB) in an aqueous solution. The photocatalytic degradation reaction was carried out in a 1 cm spectrometric quartz cuvette containing 2 mL of 10 mg L^{-1} or 1 mg L^{-1} of RhB and the photocatalyst at different catalyst/RhB ratios. The RhB aqueous solution was irradiated under visible light irradiation without stirring at room temperature in air through with a cut off filter (λ = 420 nm, to suppress the light with wavelength shorter than 420 nm) using a visible fiber lamp (Spot Light Source 400–700 nm, L9566-03, Hamamatsu, Japan). The intensity of the light was measured using a PM600TM Laser Fiber Power Meter (Coherent Inc., USA) and was determined as being 0.5 W cm^{-2}. The whole quartz cuvette was directly transferred at different irradiation time intervals in a UV–vis spectrophotometer. The concentration of RhB was determined by monitoring the changes in the absorbance maximum at ca. 554 nm.

2.4. Instrumentation

2.4.1. UV–vis spectrometry

Absorption spectra were recorded using a Perkin-Elmer Lambda UV-vis 950 spectrophotometer in a spectrometric quartz cuvette with an optical path of 10 mm. The wavelength range was 400–800 nm.

2.4.2. Raman spectroscopy

The sample for the Raman analysis was prepared by dispersing AuNPs@Mo–GO in ethanol by sonication. 50 μL of the sample was drop casted on a cleaned silicon wafer and dried. Raman analyses were performed on an HR 800 Raman spectrometer (Jobin Yvon, Horiba, France) using 632.8 nm green laser (NRS1500 W).

2.4.3. Transmission electron microscopy

High resolution transmission electron microscope (HRTEM) images were taken by using Icon analytical 300 keV microscope.

2.4.4. X-ray photoelectron spectroscopy

The initial GO and AuNPs@Mo–GO were deposited as thin films on clean p-type (1 0 0) silicon wafers by casting 50 μL of the respective suspension and removal of water by drying the substrates on a heating plate at 70 °C in air. X-ray photoelectron spectroscopy (XPS) measurements were performed with an ESCALAB 220 XL spectrometer from Vacuum Generators featuring a monochromatic Al Kα X-ray source (1486.6 eV) and a spherical energy analyzer operated in the CAE (constant analyzer energy) mode (CAE = 100 eV for survey spectra and CAE = 40 eV for high-resolution spectra), using the electromagnetic lens mode. No flood gun source was needed due to the conducting character of the substrates. The angle between the incident X-rays and the analyzer is 58°. The detection angle of the photoelectrons is 30°. Fitting was made using CasaXPS 2.3.16Dev37 software using Gaussian Lorentzian shape GL(30) curves.

3. Results and discussion

Fig. 1 displays the strategy for the preparation of AuNPs@Mo–GO nanocomposite. GO nanosheets investigated in this work are prepared by the modified Hummer's method from natural graphite powder [14]. In a typical procedure, an aqueous solution of GO (600 μL, 1.5 mg mL^{-1}), $Na_2[Mo_6Br_8(N_3)_6]$ (600 μL, 1 mM), $HAuCl_4{\cdot}3H_2O$ (600 μL, 1.5 mM), and isopropanol (4 μL) was irradiated at λ = 365 nm (power intensity = 0.5 W cm^{-2}) for 30 min at room temperature in air using a UV fiber lamp. The AuNPs@Mo–GO material was separated from the solution by centrifugation (14 000 rpm for 20 min). The product was washed with water several times and resuspended in water at a concentration of 1 mg mL^{-1}.

Fig. 2a exhibits UV–vis absorption spectra of the starting GO and AuNPs@Mo–GO nanocomposite. No obvious absorption band in the wavelength range of 400–800 nm can be seen from GO. In contrast, the UV–vis spectrum of the AuNPs@Mo–GO nanocomposite displays an absorption peak at ~540 nm due to the plasmonic band of the Au NPs of 10–20 nm in diameter, suggesting the formation of AuNPs on the surface of GO sheets. Moreover, the initial brown color of the nanocomposite dispersion turned to purple brown during the irradiation process, indicating the formation of AuNPs. Fig. 2b shows the Raman spectrum of the as-synthesized material. The Raman shifts at 1322 cm^{-1} and 1586 cm^{-1} are the characteristic D- and G-bands of the GO, respectively, where the D-band is the breathing mode of κ-point phonons of A_{1g} symmetry due to the local defects and disorder at the edges of the GO and the G-band is due to E_{2g} phonon of sp^2 C atoms [18,19]. The Raman shift at 867 cm^{-1} is most likely due to the asymmetric stretching mode of the terminal Mo=O bond [20].

Transmission electron microscopy (TEM) measurements were performed to characterize the morphology of the as-synthesized AuNPs@Mo–GO nanocomposite material. GO displays sheets with chiffon-like wrinkles as shown in Fig. 3a. It clearly shows the presence of spherical AuNPs with a mean diameter of 16 ± 9 nm (see inset, dark particles), and amorphous molybdenum clusters

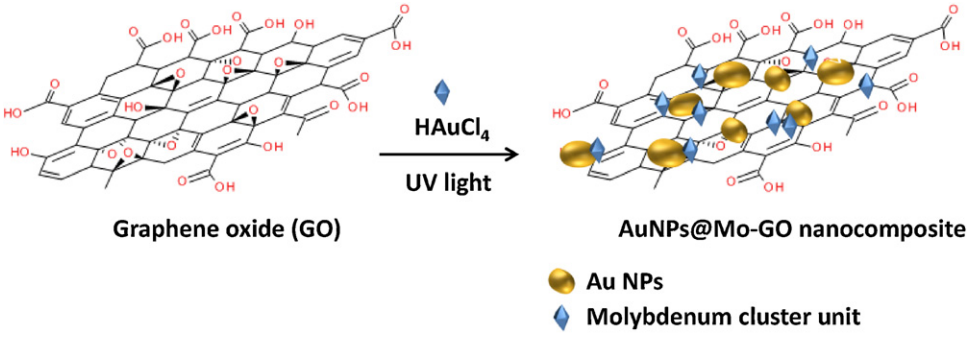

Fig. 1. Schematic representation of one pot synthesis of AuNPs@Mo–GO nanocomposite.

with a mean diameter of 54 ± 15 nm (see inset, light particles) anchored onto the GO sheets. The position of the plasmonic band (Fig. 2a) is in accordance with the TEM results. Fig. 3b depicts an HRTEM image of a single Au nanoparticle in the composite material. It shows lattice fringes of the AuNPs with a d-spacing value of 0.234 nm, which corresponds to the Au (1 1 1) plane [21,22]. Selected area electron diffraction pattern of the AuNPs@Mo–GO composite material is displayed in Fig. 3c. The six bright spots on the ring correspond to the GO and the rings 1 and 2 correspond to the Au (1 1 1) and Au (2 0 0) planes, respectively. EDX analysis of the AuNPs@Mo–GO composite material also confirms the presence of signals due to C, O, Mo, and Au atoms (Fig. 3d). The presence of Cu originates from the copper TEM grid. Other elements such as Na and Br overlap with the Cu and Au signals.

For X-ray photoelectron spectroscopy (XPS) characterization, the initial GO and AuNPs@Mo–GO were deposited as thin films on clean p-type (1 0 0) silicon wafers by casting 50 μL of the respective suspension and removal of water by drying the substrates on a heating plate at 70 °C in air. XPS survey spectrum of the starting GO reveals characteristic peaks at 285 and 533 eV due to C 1s and O 1s, respectively, in accordance with the chemical composition of GO, and a small peak at 402 eV due to N 1s (Fig. 4a). The latter peak is most likely due to surface contamination during GO preparation. After UV irradiation in the presence of $HAuCl_4{\cdot}3H_2O$ and $Na_2[Mo_6Br_8(N_3)_6]$, additional peaks due to Mo 3p (395.2 eV), Mo 3d (229.3 eV), Br 3p (183.6 eV), Br 3d (68.7 eV) and Au 4f (84.1 eV) are seen in the spectrum in accordance with the chemical composition of the nanocomposite (Fig. 4b). The experimental ratio between the atomic concentrations of Mo and Br is estimated to be 0.80, which is very close to the theoretical value of 0.75 (6Mo/8Br), in agreement with the original structure of the molybdenum cluster.

High resolution C 1s XPS spectra of the GO before and after UV irradiation in the presence of $HAuCl_4{\cdot}3H_2O/Na_2[Mo_6Br_8(N_3)_6]$ are comparable, suggesting that the structure of the initial GO remained intact (no reduction of GO to graphene) during this process (Fig. 5a and b). The C1s XPS core level spectrum of GO is displayed in Fig. 5a. It can be deconvoluted into four components with binding energies at 284.9, 286.9, 288.3 and 290.9 eV. The peak located at the binding energy of 284.9 eV was attributed to the C—C, C═C, and C—H bonds. The higher binding energy peaks at 286.9, 288.3 and 290.9 eV are attributed to carbon species of higher oxidation states C—O, C═O, and O═C—O species, respectively [23–25]. The Mo 3d peak displays two bands at 229.3 and 232.4 eV due to Mo $3d_{5/2}$ and Mo $3d_{3/2}$, respectively (Fig. 5c) [22]. The position of the Mo $3d_{5/2}$ and $3d_{3/2}$ peaks is perfectly consistent with a Mo^{II} oxidation state. A small doublet at 232.4 and 235.2 eV due to Mo^{VI} $3d_{5/2}$ and Mo^{VI} $3d_{3/2}$, respectively is also detected, most likely due to the slight oxidation of the molybdenum cluster [26]. The Au_{4f} XPS spectrum of AuNPs@Mo–GO shows two major peaks at 84.1 eV due to $Au_{4f7/2}$ and at 87.8 eV due to $Au_{4f5/2}$, similar to $Au^0{}_{4f7/2}$ (84.0 eV) and $Au^0{}_{4f5/2}$ (87.7 eV), which are characteristic for metallic Au^0 [27], and additional shoulders at 85.2 and 88.8 eV due to $Au^+{}_{4f7/2}$ and $Au^+{}_{4f5/2}$, respectively (Fig. 5d). The XPS result suggests that most of the Au species are present in the metallic form.

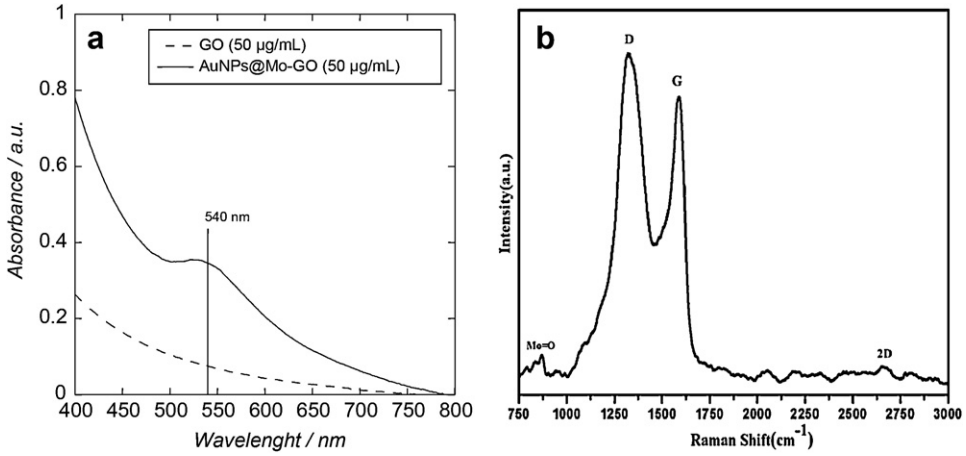

Fig. 2. (a) UV–vis absorption spectra of the AuNPs@Mo–GO in comparison with the starting GO solution; (b) Raman spectrum of the AuNPs@Mo–GO composite material.

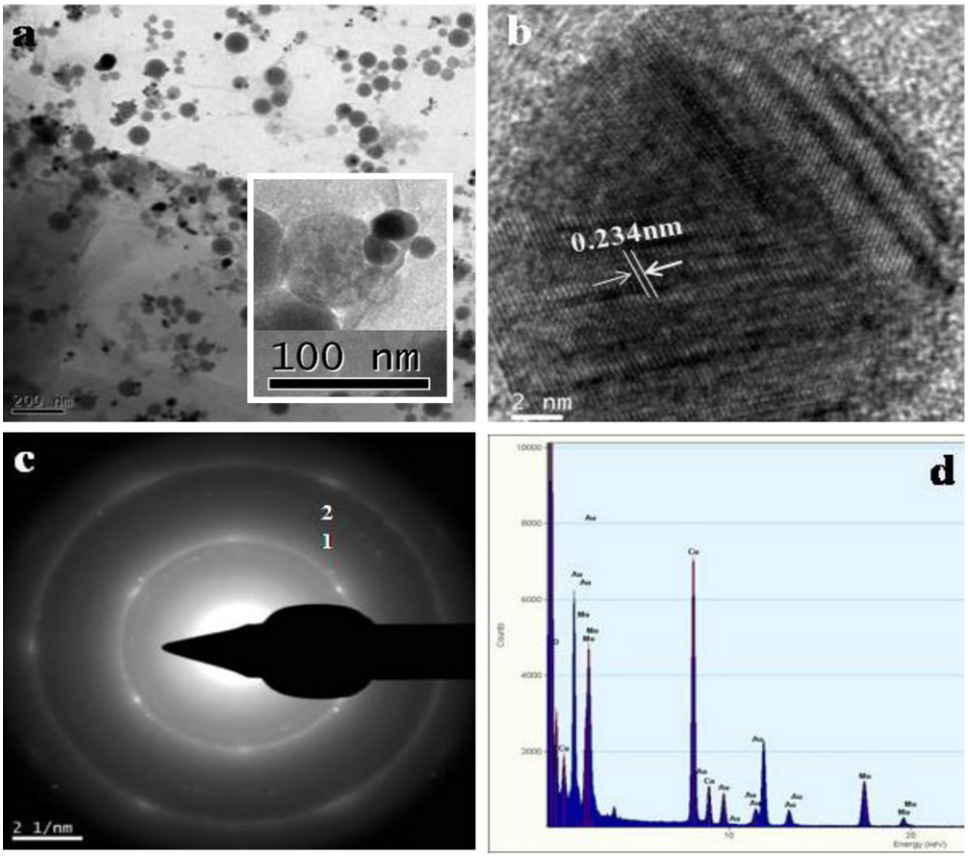

Fig. 3. (a) TEM image of the AuNPs@Mo–GO composite, (b) HRTEM image of a Au particle in the composite material, (c) SAED pattern, (d) EDX spectrum of the AuNPs@Mo–GO composite material.

The photodegradation of rhodamine B (RhB), as the model of organic pollutant, by AuNPs@Mo–GO was evaluated under visible light irradiation ($\lambda > 420$ nm; power = 0.5 W cm^{-2}). The photodegradation was carried out at room temperature by addition of the nanocomposite material into a 2 mL aqueous solution of RhB with an initial concentration of 10 mg L^{-1} (Fig. 6a and c) and 1 mg L^{-1} (Fig. 6b and d). An aqueous solution of RhB displays a strong and characteristic absorption band at 554 nm. The photocatalytic degradation was monitored by the decay of the absorption of RhB as a function of irradiation time. RhB was very stable under visible light irradiation in the absence of catalyst. Similarly, direct irradiation of RhB over GO showed less than 10% degradation after 120 min under visible light irradiation under otherwise identical experimental conditions. The results suggest that GO alone is not efficient for the photodegradation of RhB. Fig. 6 exhibits UV–vis spectra of RhB (initial concentration = 10 mg L^{-1}) before and after visible light irradiation in the presence of AuNPs@Mo–GO at 10 mg L^{-1} (catalyst/RhB ratio = 1:1). The degree of degradation is about 80% after 120 min irradiation. Decreasing the catalyst/RhB ratio from 1:1 to 0.5:1 showed a significant decrease of the photocatalytic performance of the catalyst. Indeed, only 42% of RhB was decomposed after 120 min irradiation (Fig. 6c). Fig. 6b shows UV–vis absorption spectra of RhB (1 mg L^{-1}) before and after visible light irradiation in the presence of 2.5 mg L^{-1} of AuNPs@Mo–GO photocatalyst. An almost complete decolorization of RhB was observed after 100 min irradiation. Further increase of catalyst concentration to 5 mg L^{-1} (catalyst/RhB ratio = 5:1) did not show any increase of the decomposition rate, suggesting that the optimal ratio is around 2.5:1 and a saturation effect is observed above this concentration (Fig. 6d). The results obtained using AuNPs@Mo–GO nanocomposite as photocatalyst indicate a higher performance for this catalyst, as compared to RGO–TiO_2 and RGO–SnO_2 photocatalysts [11].

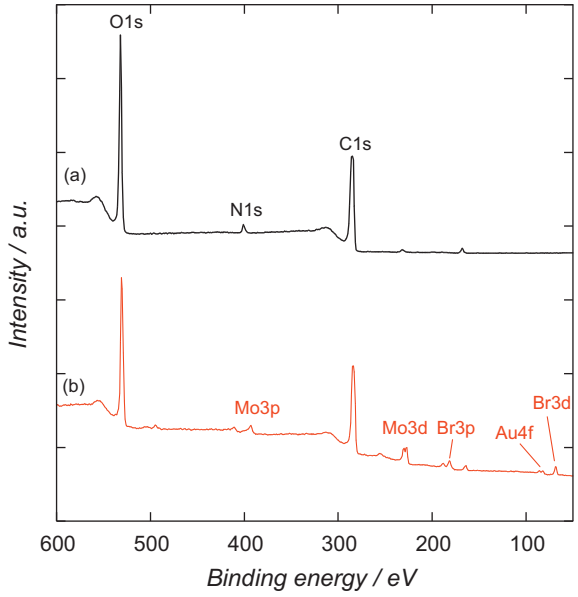

Fig. 4. High resolution XPS spectra of the starting GO (a) and AuNPs@Mo–GO (b).

The activity and stability of AuNPs@Mo–GO nanocomposite were further investigated by recycling runs. After each run, a fresh

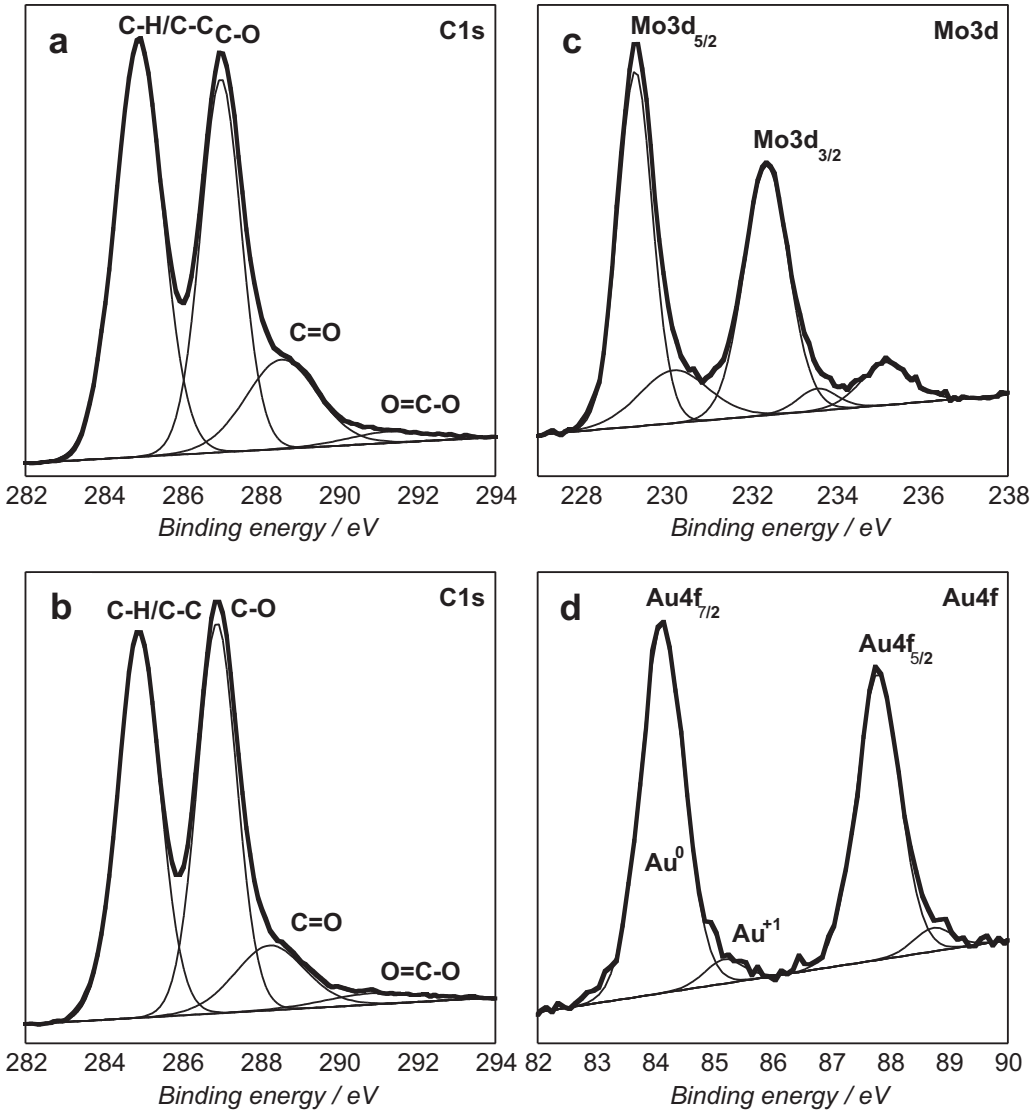

Fig. 5. (a) C 1s core level XPS spectrum of the starting GO; C 1s (b), Mo 3d (c), and Au 4f (d) core level XPS spectra of AuNPs@Mo–GO.

concentrated solution of RhB (2 μg/run) was added to obtain the initial concentration of RhB (1 mg L^{-1}) without causing a significant dilution. RhB photodegradation in the presence of 2.5 mg L^{-1} of AuNPs@Mo–GO photocatalyst is almost complete within ~60 min under visible light irradiation (Fig. 7). Furthermore, the photocatalyst remains active under visible light irradiation without any loss of its performance after six successive runs.

A plausible mechanism for the photocatalytic degradation of RhB in the presence of AuNPs@Mo–GO can be summarized as follows:

$$[\text{Mo cluster}] \xrightarrow{h\nu} [\text{Mo cluster}]^* \quad \text{i.e.} \quad [\text{Mo cluster}](h^* + e^-) \qquad (1)$$

$$[\text{Mo cluster}](h^+ + e^-) + H_2O \rightarrow [\text{Mo cluster}](e^-) + HO^\bullet + H^+ \qquad (2)$$

$$HO^\bullet + \text{RhB} \rightarrow \text{oxidation products} \rightarrow\rightarrow CO_2 + H_2O + \text{inorganic ions}$$

An electron–hole pair is generated upon excitation of the composite with a photon of energy equal to or higher than the band gap of the [Mo cluster] ($E_g \sim 2.1$ eV) [3]. Reaction of the photoexcited catalyst with H_2O (i.e. oxidative hole trapping) creates "surface" bound OH radicals (Eqs. (1)–(2)). The hydroxyl radicals react subsequently with RhB in various ways such hydroxylation, H-abstraction, and oxidation products.

Dioxygen is a very effective oxidant for reduced [Mo cluster], thus its main action is the regeneration of the catalyst (Eq. (3)). The formation of superoxide radical anion $O_2^\bullet$ ($O_2^\bullet + H^+ \leftrightarrow HO_2^\bullet$) may participate further in oxidative as well as reductive processes (Eq. (4)).

$$[\text{Mo cluster}](e^-) + O_2 \rightarrow [\text{Mo cluster}] + O_2{}^{-\bullet} \qquad (3)$$

$$O_2{}^{-\bullet}/HO_2^\bullet + S \rightarrow \text{oxidation products} \qquad (4)$$

Because of the low photocatalytic activity of GO alone, we believe that its role in the photocatalytic process is to favor RhB adsorption on the nanohybrid surface via π–π stacking. The Au NPs on the other hand are expected to participate in the photocatalytic process by enhancing charge separation. However, it is not excluded that RhB degradation is mainly due to a photosensitization process rather than direct excitation of the nanohybrid [11]. Further experiments using small molecules without any absorption features in the visible range will help elucidating the mechanism.

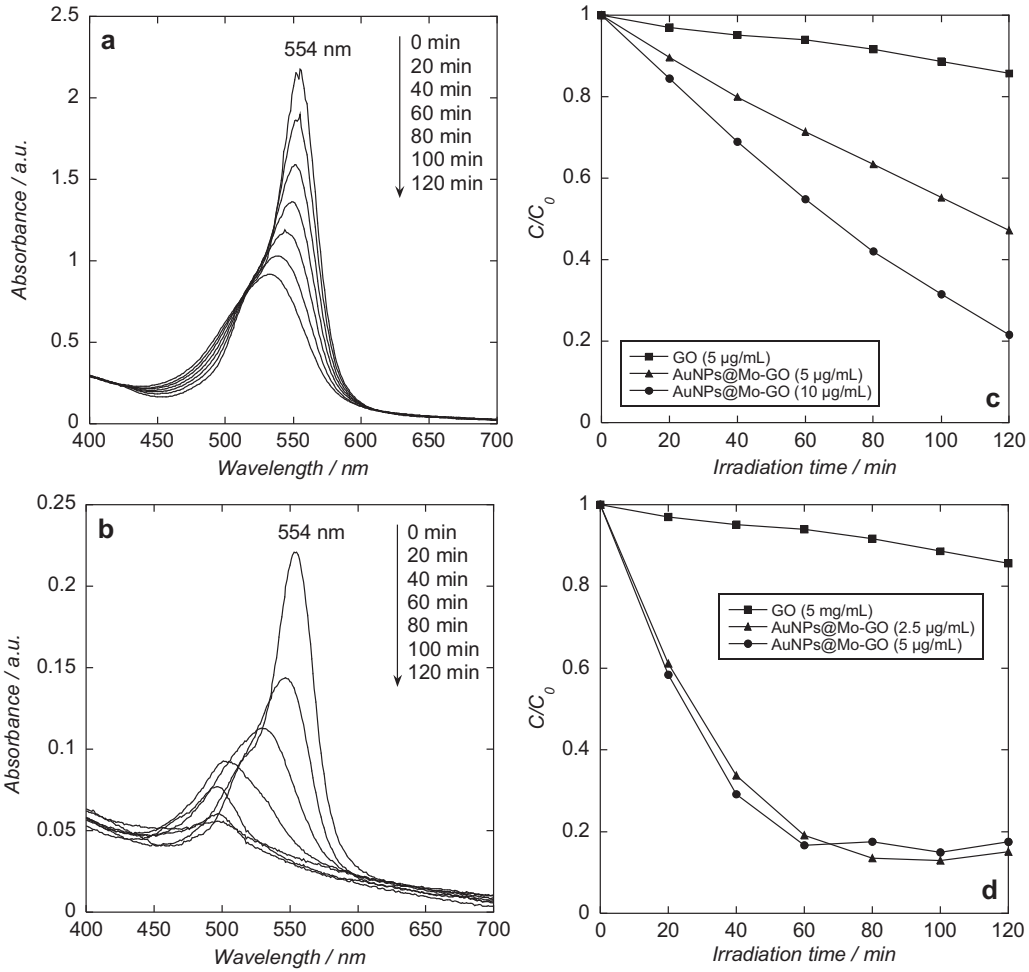

Fig. 6. UV–vis absorption spectra of RhB before and after irradiation in the presence of AuNPs@Mo–GO composite as a function of irradiation time under visible light irraditation with catalyst/RhB ratio 1:1 (a) and 2.5:1 (b); temporal course of the photocatalytic degradation of RhB at 10 mg L^{-1} (c) and at 1 mg L^{-1} (d) with different concentrations of AuNPs@Mo–GO under visible light irradiation.

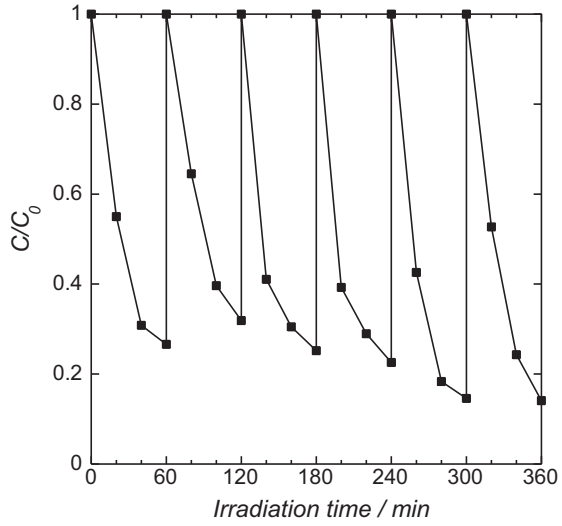

Fig. 7. Cycling experiments in the photocatalytic degradation of rhodamine B in the presence of AuNPs@Mo–GO composite at 2.5 mg L^{-1} under visible light irradiation. The initial concentration of rhodamine B is 1 mg L^{-1}, the addition of rhodamine B is 2 μg/run.

4. Conclusion

In summary, a facile and versatile synthetic route for the preparation of AuNPs@GO–Mo nanocomposite is reported. The technique relies on the UV irradiation of GO in the presence of $Na_2[Mo_6Br_8(N_3)_6]$ and $HAuCl_4{\cdot}3H_2O$. The resulting material showed excellent photocatalytic performance for the degradation of rhodamine B under visible light irradiation. The technique reported herein can be easily generalized to other types of metal nanoparticles and holds promise in view of various photocatalytic applications of the resulting nanocomposite materials.

Acknowledgements

The Centre National de la Recherche Scientifique (CNRS), the European Community (FEDER), the Nord Pas de Calais region, and the Université Lille 1 Sciences et Technologies are gratefully acknowledged for financial support.

References

[1] E. Forgacs, T. Cserhati, G. Oros, Environment International 30 (2004) 953.
[2] M.R. Hoffmann, S.T. Martin, W.Y. Choi, D.W. Bahnemann, Chemical Reviews 95 (1995) 69.
[3] A. Barras, S. Cordier, R. Boukherroub, Applied Catalysis B: Environmental 123–124 (2012) 1.
[4] A.W. Maverick, J.S. Najdzionek, D. MacKenzie, D.G. Nocera, H.B. Gray, Journal of the American Chemical Society 105 (1983) 1878.

[5] J.A. Jackson, C. Turro, M.D. Newsham, D.G. Nocera, Journal of Physical Chemistry 84 (1990) 4500.
[6] S. Cordier, K. Kirakci, D. Méry, C. Perrin, D. Astruc, Inorganica Chimica Acta 359 (2006) 1705.
[7] S. Park, R.S. Ruoff, Nature Nanotechnology 4 (2009) 217.
[8] D.R. Dreyer, S. Park, C.W. Bielawski, R.S. Ruoff, Chemical Society Reviews 39 (2010) 228.
[9] I. Kaminska, A. Barras, Y. Coffinier, W. Lisowski, J. Niedziolka-Jonsson, P. Woisel, J. Lyskawa, M. Opallo, A. Siriwardena, R. Boukherroub, S. Szunerits, ACS Applied Materials & Interfaces 4 (2012) 5386.
[10] B.F. Machado, P. Serp, Catalysis Science & Technology 2 (2012) 54.
[11] J. Zhang, Z. Xiong, X.S. Zhao, Journal of Materials Chemistry 21 (2011) 3634.
[12] Z. Xiong, L.L. Zhang, J. Ma, X.S. Zhao, Chemical Communications 46 (2010) 6099.
[13] D. Bublitz, W. Preetz, M.K.Z. Simsek, Zeitschrift für anorganische und allgemeine Chemie 623 (1997) 1.
[14] M.R. Das, R.K. Sarma, R. Saikia, V.S. Kale, M.V. Shelke, P. Sengupta, Colloids Surfaces B: Biointerfaces 83 (2011) 16.
[15] O. Fellahi, M.R. Das, Y. Coffinier, S. Szunerits, T. Hadjersi, M. Maamache, R. Boukherroub, Nanoscale 3 (2011) 4662.
[16] I. Kamińska, M.R. Das, Y. Coffinier, J. Niedziółka-Jönsson, P. Woisel, M. Opałło, S. Szunerits, R. Boukherroub, Chemical Communications 48 (2012) 1221.
[17] I. Kamińska, M.R. Das, J. Niedziółka-Jönsson, P. Woisel, J. Lyskawa, M. Opałło, R. Boukherroub, S. Szunerits, ACS Applied Materials & Interfaces 4 (2012) 1016.
[18] K.N. Kudin, B. Ozbas, H.C. Schniepp, R.K. Prud'homme, I.A. Aksay, R. Car, Nano Letters 8 (2008) 36.
[19] S. Stankovich, D.A. Dikin, R.D. Piner, K.A. Kohlhaas, A. Kleinhammes, Y. Jia, Y. Wu, S.T. Nguyen, R.S. Ruoff, Carbon 45 (2007) 1558.
[20] T. He, J.N. Yao, Journal of Photochemistry and Photobiology C 4 (2003) 125.
[21] Y.-C. Cheng, C.-C. Yu, T.-Y. Lo, Y.-C. Liu, Materials Research Bulletin 47 (2012) 1107.
[22] S. Ababou-Girard, S. Cordier, B. Fabre, Y. Molard, C. Perrin, Chemphyschem 8 (2007) 2086.
[23] D. Yang, A. Velamakanni, G. Bozoklu, S. Park, M. Stoller, R. Piner, S. Stankovich, I. Jung, D. Field, C.A. Ventrice Jr., R.S. Ruoff, Carbon 47 (2009) 145.
[24] O. Akhavan, E. Ghaderi, Journal of Physical Chemistry C 113 (2009) 20214.
[25] O. Akhavan, ACS Nano 4 (2010) 4174.
[26] Y.-J. Lee, D. Barrera, K. Luo, J.W.P. Hsu, Journal of Nanotechnology 2012 (2012) 195761.
[27] R. Leppelt, B. Schumacher, V. Plzak, M. Kinne, R.J. Behm, Journal of Catalysis 244 (2006) 137.